Thermal behavior and decomposition of cerium(III) butanoate, pentanoate and hexanoate salts upon heating in argon

Grivel, Jean-Claude; Suarez Guevara, Maria Josefina; Yue, Zhao; Tang, Xiao; Pallewatta, Pallewatta G A P; Bednarcik, J.

Published in:
Journal of Analytical and Applied Pyrolysis

Link to article, DOI:
10.1016/j.jaap.2017.06.022

Publication date:
2017

Document Version
Peer reviewed version

Thermal behavior and decomposition of cerium(III) butanoate, pentanoate and hexanoate salts upon heating in argon

J.-C. Grivel[1,], M.J. Suarez Guevara[1], Y. Zhao[1,2], X. Tang[1,3], P.G.A.P Pallewatta[1,4], J. Bednarčík[5] and A. Watenphul[6]*

[1]Department of Energy Conversion and Storage, Technical University of Denmark, 4000 Roskilde Denmark

[2]Department of Electrical Engineering, Shanghai Jiao Tong University, Shanghai 200240, Peoples R. China

[3]Institute of Physical Chemistry, University of Hamburg, Grindelallee 117, 20146 Hamburg, Germany / The Hamburg Centre for Ultrafast Imaging (CUI), Luruper Chaussee 149, 22761 Hamburg, ,Germany

[4]Faculty of Computing and Technology, University of Kelanya, Sri Lanka

[5]Deutsches Elektronen-Synchroton DESY, Notkestr. 85, 22603 Hamburg, Germany

[6]Institute of Mineralogy and Petrography, University of Hamburg, Grindelallee 48, 20146 Hamburg, Gremany

***Corresponding author:** email: jean@dtu.dk

tel: +45 4677 4739

Highlights

- The thermal decomposition of cerium butanoate, pentanoate and hexanoate has been studied in Ar.
- All compounds present transitions including melting prior to decomposition.
- Gas release in the molten state results in irregular mass loss.
- CO_2 and symmetrical ketones are the main evolving gas species.
- $Ce_2O(C_nH_{2n+1}CO_2)_4$ and $Ce_2O_2CO_3$ intermediate are detected before CeO_2 formation

Abstract

The thermal behavior and decomposition of Ce-butanoate monohydrate ($Ce(C_3H_7CO_2)_3 \cdot H_2O$), Ce-pentanoate ($Ce(C_4H_9CO_2)_3$) and Ce-hexanoate ($Ce(C_5H_{11}CO_2)_3$) were studied in a flow of argon while heating at 5 °C/min. By means of several techniques such as simultaneous TG-DTA, FTIR evolved gas analysis, in-situ x-ray diffraction using a synchrotron source and hot-stage microscopy, it was found that all three compounds undergo melting transitions prior to decomposition and that decomposition involves intermediate stages including at least a $Ce_2O(C_nH_{2n+1}CO_2)_4$ intermediate (n = 3, 4 or 5 for Ce-butanoate, pentanoate or hexanoate respectively). The final decomposition product consists of CeO_2, which is formed through a Ce-oxycarbonate. The $Ce^{3+} \rightarrow Ce^{4+}$ oxidation seems to proceed via Ce_2O_3 that first results from the

decomposition of the oxycarbonate phase. During the whole decomposition process, the evolved gas species consist of CO_2 and symmetrical ketones.

Keywords: cerium; butyrate; valerate; caproate; thermal decomposition; CeO_2

1. Introduction

Due to its outstanding properties, CeO_2 has tremendous potential for exploitation in various fields including biomedical applications (biosensing, immunoassay, drug delivery, radiation protection, tissue engineering, ophthalmology, implant coatings and antioxidant usage) [1-6], photocatalysis [7], steam reforming [8], preferential oxidation of impurities and pollutants (CO [9], SO_2, NO_x [10]), fuel cells and automotive applications [11], buffer layer coatings for superconducting tapes [12,13], etc.

The synthesis of CeO_2 nanoparticles and/or coatings can be achieved via different routes such as solvothermal [14], hydrothermal [15], precipitation [16-18] or thermal decomposition of complex precursors [19-21]. For the application of the latter technique, a good knowledge of the decomposition process is highly advantageous in order to control the morphology of the coating or nanoparticles as well as for ensuring safety during large scale handling due to the evolution of potentially toxic gases. Numerous studies have been published on the thermal decomposition of various cerium carboxylate salts as will be discussed in section 3.4. Among this class of metalorganic compounds, the linear chain alkanoates have received limited attention. Besides cerium formate [22,23] and cerium acetate [24,25], the thermal decomposition of longer chain cerium alkanoates is limited to a few studies on cerium propionate [26,27], butanoate [28], pentanoate [29], hexanoate [30] and octanoate [30] performed under various conditions that do not allow systematic comparisons. Besides, there are some older works on Ce-laurate, palmitate and stearate [31] as well as hexanoate [28] that are based solely on thermogravimetric data with poor resolution (one point every 20°C), from which limited information can be obtained. The aim of

the present work was to systematically study the thermal decomposition of cerium butanoate, pentanoate and hexanoate under fixed conditions to study their thermal behavior, find similarities as well as differences between them and compare the results with those previously published on other cerium carboxylates and rare-earth butanoates, pentanoates and hexanoates.

2. Experimental

200 mg aliquots of $Ce_2(CO_3)_3 \cdot xH_2O$ ($x \approx 4$) from Alfa Aesar (99.9 % purity (rare earth basis)) were dissolved separately in excess (4 ml) butanoic acid (Alfa Aesar, 99+%, common name: butyric acid), pentanoic acid (Alfa Aesar, 99 %, common name: valeric acid) or hexanoic acid (Alfa Aesar, 98+ %, common name: caproic acid). After slow evaporation at room temperature for the solution in butanoic acid or 60°C for the other two solutions during several weeks without stirring, a hard, yellow, transparent layer had formed on the bottom of the glass beakers. This mass was mechanically extracted and crushed into powders that were used without further treatment for characterisation and for the thermal decomposition studies.

Simultaneous thermogravimetry (TG) and differential thermal analysis (DTA) traces were acquired in a STA 449C Netzsch device at a heating rate of 5 °C/min up to 1000°C in an argon flow of 40 ml/min at atmospheric pressure. Al_2O_3 (alumina) crucibles with 6 mm diameter and 3 mm depth were used. Buoyancy corrections were performed using background data recorded on empty crucibles under the same experimental conditions. A sample mass of 11.5 ± 0.2 mg was used for all measurements. The powders were not compacted. α-Al_2O_3 powder (46 mg) was used as reference.

Evolved gas analysis was performed by recording Fourier transform infrared (FTIR) spectra with a Bruker Tensor 27 spectrometer linked to the exhaust of the TG-DTA instrument by a transfer line maintained at 200°C to minimize condensation of volatile decomposition products. FTIR

spectra were also recorded on samples heated in the TG-DTA apparatus at a rate of 5 °C/min and air quenched by opening the furnace in order to follow the evolution of the decomposition products. High-temperature hard x-ray (synchrotron) diffraction measurements up to 560°C were conducted at the Wiggler beamline BW5, located at the storage ring DORIS at DESY in Hamburg (Germany). The diffraction patterns were recorded during a temperature ramp of 5 °C/min with Ar flow in a dedicated furnace. The photon energy of the incident beam was 100 keV, corresponding to a wavelength $\lambda = 0.124$ Å. Details on the experimental setup and data analysis can be found in previous publications [32,33]. The advantage of using high-energy X-rays over a conventional laboratory X-ray source for this in-situ study is that the exposure time for each complete pattern can be as short as one second, thus avoiding averaging over a large temperature interval. The evolution of microstructural features was observed in-situ at low magnification (50x) by hot-stage optical microscopy up to 600°C with a heating rate of 5 °C/min under Ar flow in a HCP901 chamber from INSTEC Ltd calibrated by observing the melting of metal standards (In, Sn, Bi, Zn and Al).

3. Results and discussion

3.1 Ce-hexanoate

The FTIR spectrum of the dried powder is shown in Fig.1. It includes all the absorption bands previously observed in Ce-hexanoate [34], Y-hexanoate [35] and La-hexanoate [36], while the characteristic strong absorption bands for Ce-acetate at 1017 cm^{-1} and 1054 cm^{-1} [37] are not apparent, which allows concluding that the obtained compound consists of Ce-hexanoate. This is further supported by the similarity of the XRD pattern features (31°C in Fig.2) with those of La-hexanoate [36] as well as by the good fit between the theoretical mass loss corresponding to the decomposition of Ce-hexanoate into CeO_2 (64.5 %) and the experimental result of thermal

decomposition (64,0 %) as will be shown in the following. The absence of a broad FTIR band between 3500 cm^{-1} and 3000 cm^{-1} indicates that the Ce-hexanoate salt has been obtained in the anhydrous state (Fig.1). The separation between the $\nu_{as}(COO^-)$ and $\nu_s(COO^-)$ absorption bands ($\Delta\nu(COO)$) amounts to 131 cm^{-1}. This value is in the same range as for the cerium alkanoates investigated by Marques et al. [39] and Jongen et al. [40]. It is on the other hand smaller than for the ionic Na-hexanoate compound (145 cm^{-1}) [41]. According to Deacon and Phillips [42], this points to bidentate chelating but more than a single coordination type might be present as discussed in [40].

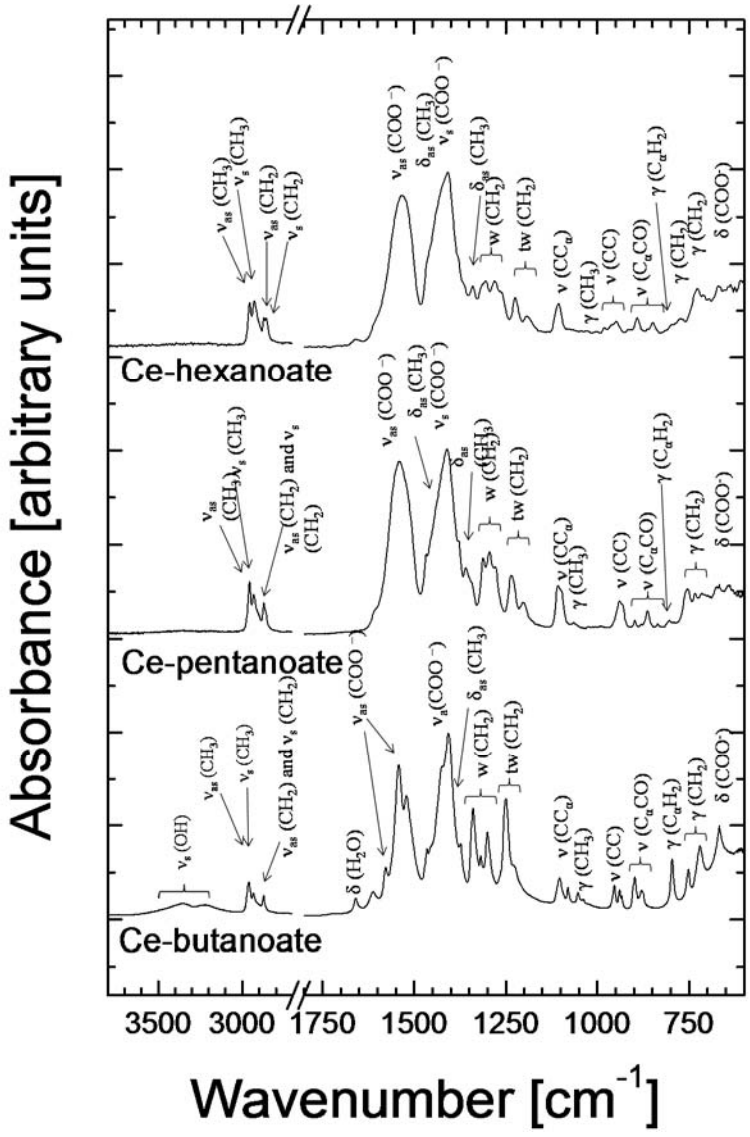

Figure 1: FTIR spectrum of the as-prepared Ce-hexanoate, Ce- pentanoate and Ce-butanoate samples with band assignments based on [35,36,38,46].

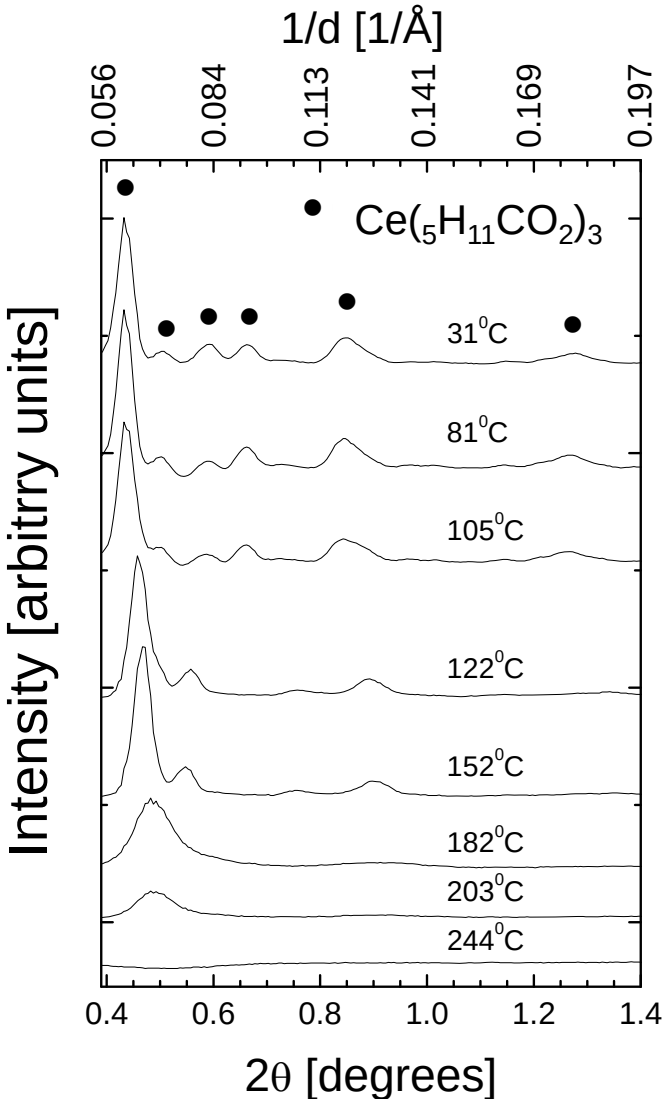

Figure 2: In-situ high energy (synchrotron) XRD patterns recorded during heating Ce-hexanoate powders at 5°C/min in Ar.

Fig. 3 shows the DTA, TG and DTG traces of Ce-hexanoate powders. In the low temperature part of the DTA trace (T < 200°C), two endothermic features, noted I and II, are visible with minima at 112°C and 157°C respectively. The first of those appears in the same temperature range as the dehydration endothermic peak observed by Brzyska and Paszkowska [30] upon heating

$Ce(C_5H_{11}CO_2)_3 \cdot 2H_2O$ in air. However, since the FTIR spectrum of our starting sample does not show the presence of absorption bands related to H_2O, the endothermic peak I visible in Fig. 2a must be related to another cause. It more probably corresponds to a liquid crystalline phase transition reported by Jongen et al [40] for the same compound. The hot-stage optical micrographs presented in Fig. 4 show that the microstructure of the powder has not significantly changed between before and after the first endothermic peak (images at 40°C, 130°C and 140°C), but it looks more shiny and the particles are no more opaque, albeit not totally transparent after the endothermic event I. In-situ synchrotron data reveal a simultaneous structural change taking place in the same temperature interval, as shown in Fig.2 (diffraction patterns at 105°C and 122°C). The sample is still crystalline, but the diffraction peaks have moved to higher 2θ values, suggesting a decrease of the lattice parameters. This is in accordance with the observations reported in [40] for the $Ce(C_nH_{2n+1}COO)_3$ $5 \leq n \leq 17$ series of Ce(III) alkanoates, where it is proposed that some kind of folding takes place in the alkyl chains, whereas the coherence of the lamellar bilayer structure based on planar Ce(III) ions layers is maintained. This transition could be a solid to smectic phase change according to the typical shift of the most intense diffraction peak that can be linked to the corresponding decrease of the interplanar lattice parameters. This is the only phase transition that could be evidenced in this sample between room temperature and 130°C, in contrast to the report of Jongen et al. [40], who mention an additional mesophase appearing before the smectic A phase. A close inspection of peak I (see inset in Fig. 3a) shows that it is asymmetric with kind of a shoulder on the low temperature side. The peak onset is estimated at 80°C and the DTA trace is back to the base line at 135°C ± 2°C. Peak I could therefore in principle encompass the two liquid crystalline phase transitions reported by Jongen et al. [40], i.e. crystalline → mesophase → smectic A taking place at 74°C and 110°C respectively, although in-situ X-ray diffraction failed to unambiguously

detect features that could be attributed to an intermediate mesophase in this temperature interval as shown in Fig.2 (patterns from 31°C to 122°C).

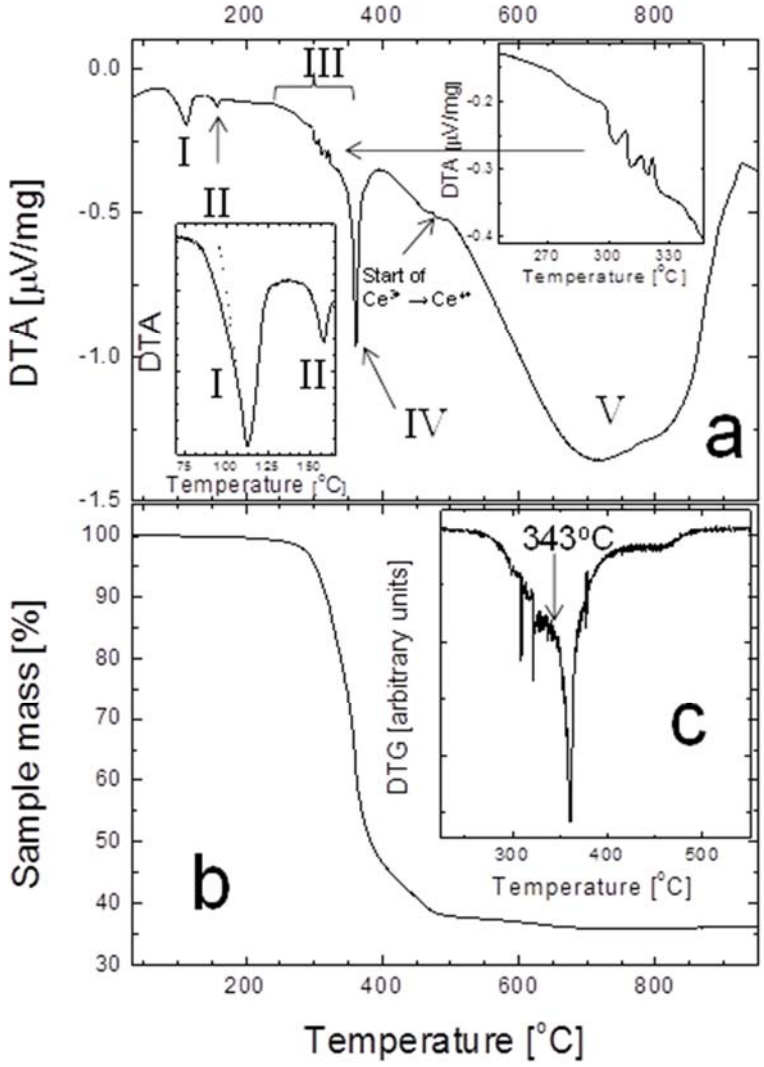

Figure 3: DTA (a), TG (b) and DTG (c) traces recorded on Ce-hexanoate upon heating at 5°C/min in Ar. Lower inset in (a): detail of the DTA trace at low temperature; upper inset in (a): magnification of the DTA trace around 300°C.

As evidenced in the optical micrographs (Fig. 4), the powders melt completely between 140°C and 160°C. Simultaneously, the crystalline reflections disappear from the diffraction patterns (Fig.2, 182°C – 244°C). This event is related to the second endothermic peak (II in Fig. 3a) and

those observations are in agreement with the smectic A to isotropic liquid reported in [40]. Fig. 2 however shows that a single broad diffraction peak centered around $2\theta = 0.5°$ ($d \approx 14.2$ Å) survives up to about 203°C, indicating that some short range order is first kept after melting but is progressively lost upon further heating. The complex composition and structure is nevertheless preserved as shown by the FTIR spectrum of a sample quenched from 190°C (Fig.5), which is similar to that of the starting powder.

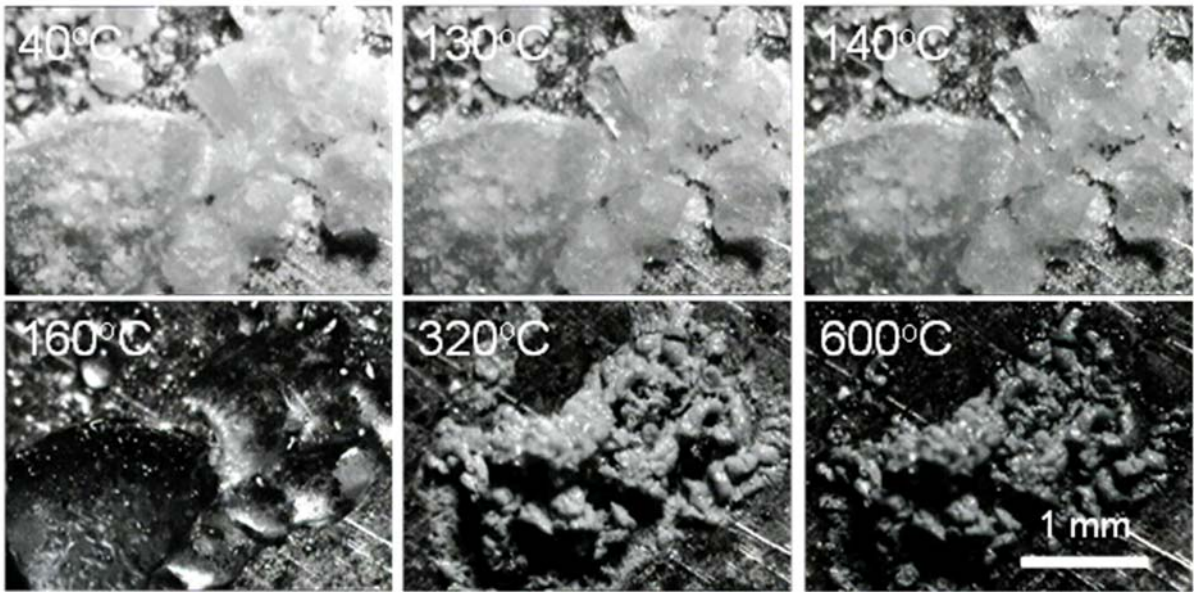

Figure 4: Hot stage optical microscope pictures taken at various temperatures during heating under Ar flow at 5°C/min on powders initially consisting of Ce-hexanoate.

At 232±3°C, a broad endothermic peak starts in the DTA trace (III in Fig.3a). It is characterized by irregular features (IV in Fig. 3a) and accompanied by a significant mass loss. At 343±5°C takes place the onset of another, this time very sharp endothermic peak (IV in Fig. 3a). The onset of this peak also marks an acceleration of the mass loss. At 343°C, the mass loss amounts to 22.1%. This would correspond very well to the formation of an intermediate $Ce_2O(C_5H_{11}CO_2)_4$ compound (theoretical mass loss = 22.1%). It is however difficult to ascertain the formation of such an intermediate compound. In the $280°C \leq T \leq 290°C$ range, the in-situ XRD patterns show the

apparition of a new, broad peak centered around 2θ = 0.5° (Fig.6a). The emergence of this low-angle diffraction peak takes place in parallel with the solidification of the sample, which is evidenced by the in-situ optical microscope image taken at 320°C shown in Fig. 4 and, which is complete around 330°C – 340°C. The new XRD peak is located at the same position as the one observed short after melting (182°C in Fig.2) and is accompanied by another broad peak at about 3.7° (285°C in Fig.6b) that was also present at 182°C (not shown in Fig. 2). However, these features weaken rapidly and disappear between 306°C and 347°C, at which temperature they are replaced by a new set of low-angle diffraction peaks becoming more prominent with increasing temperature up to 378°C (Fig.6a). These peaks disappear in turn between 380°C and 450°C.

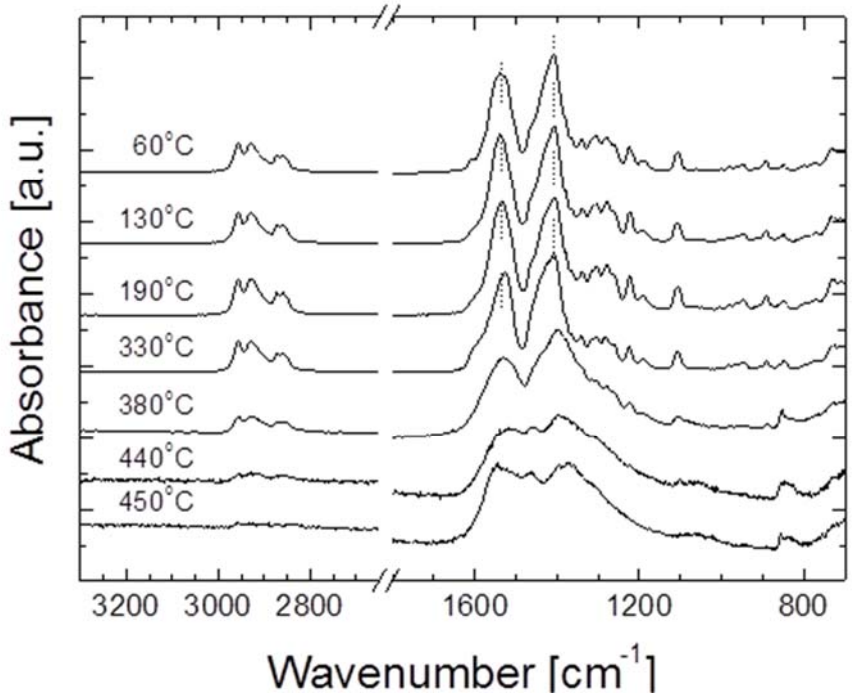

Figure 5: FTIR spectra of the solid residue quenched from various temperatures along a heating ramp of 5°C/min in an Ar atmosphere. The starting powders consisted of Ce-hexanoate.

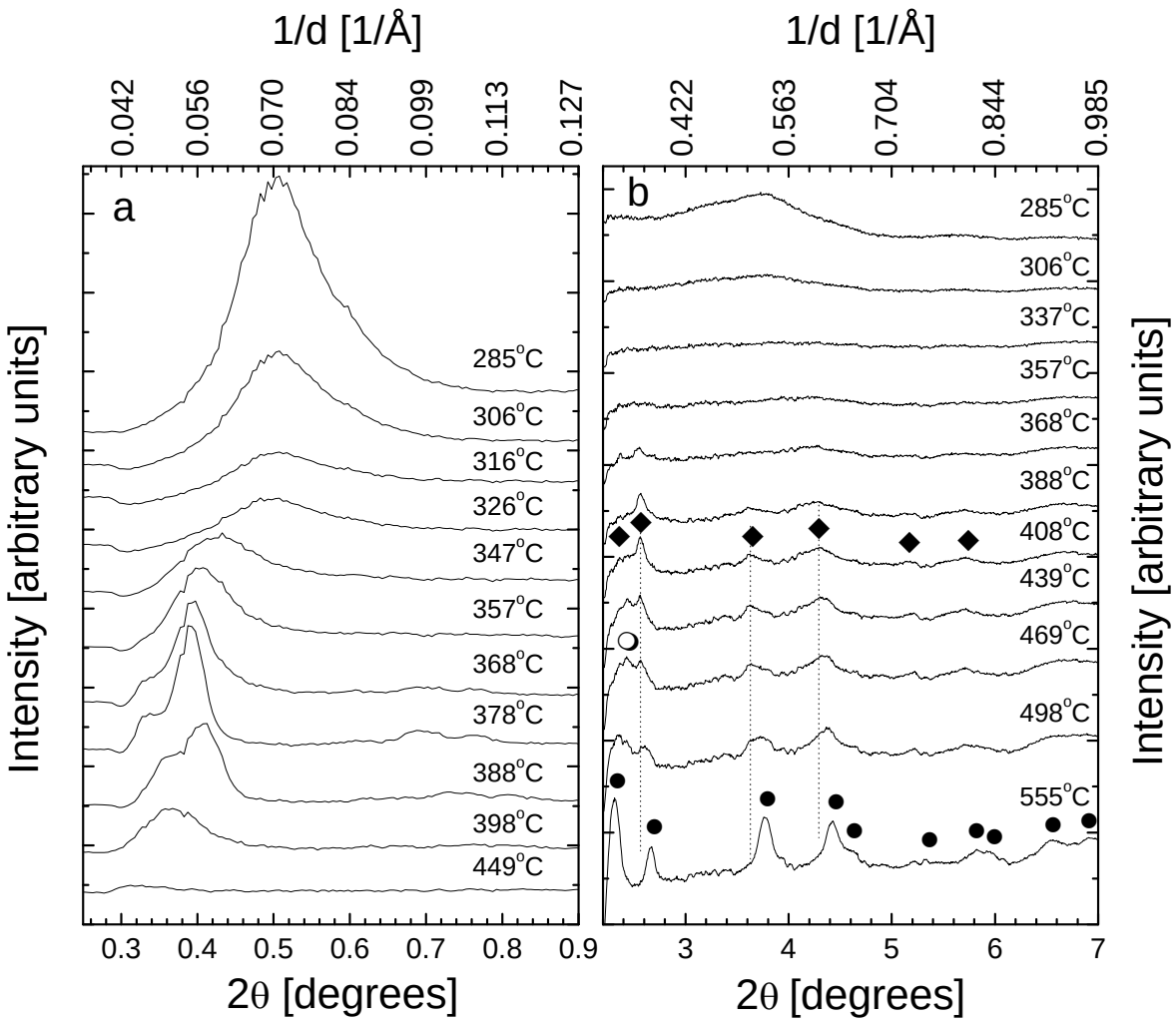

Figure 6: In-situ high energy (synchrotron) XRD patterns recorded during heating Ce-hexanoate powders at 5°C/min in Ar. A: low 2θ angle range, b: high 2θ angle range. ● CeO_2; ◆ $Ce_2O_2CO_3$; ○ Ce_2O_3.

From these observations, it can be inferred that the transformation occurring in section III of the DTA trace (Fig.3a) involves the solidification of the liquid phase, which decomposes and has been replaced by another one by about 347°C. The superimposition of the endothermic decomposition and exothermic recrystallization can be responsible for the erratic behavior of the DTA trace between 250°C and 340°C. Sudden surges in mass loss giving rise to spikes in the DTG trace (Fig.3c) between 300°C and 325°C can be ascribed to sudden releases of evolving gases when the

sample is still partly liquid, similarly to the mechanism assumed for Ba-valerate thermal decomposition [43].

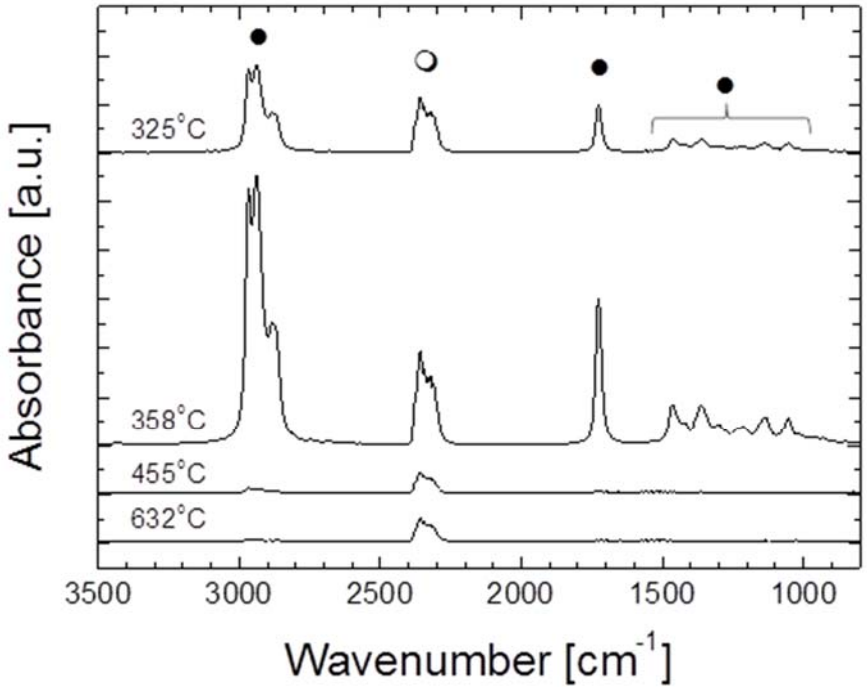

Figure 7: FTIR spectra of the gas phase evolved from Ce-hexanoate a different temperatures during thermal decomposition. ○ CO_2; ● $C_5H_{11}COC_5H_{11}$.

The analysis of the gas species evolving during stage III reveals the release of CO_2 and the symmetrical ketone 6-undecanone ($C_5H_{11}COC_5H_{11}$) as illustrated by the spectrum registered at 325°C in Fig.7. Based on these observations, the following reaction can be proposed for stage III:

$$2Ce(C_5H_{11}CO_2)_3 \rightarrow Ce_2O(C_5H_{11}CO_2)_4 + C_5H_{11}COC_5H_{11} \nearrow + CO_2 \nearrow \qquad (1)$$

A comparison of the FTIR spectra of the solid residues quenched from 190°C and 330°C (Fig.5) shows that the absorption bands due to the hexanoate ligands are preserved through the stage III reaction. However, the Δ_v(COO) value decreases from 131 cm^{-1} to 119 cm^{-1} due to the shift of the top of the ν_{as}(COO) band towards lower wavenumbers. This suggests an increase of the bidentate character of coordination at the expense of monodentate coordination contribution. This could be

expected if the relative number of hexanoate ligands decreases in comparison with that of Ce atoms and further supports the decomposition scheme (1).

Upon further heating, the rate of mass loss accelerates in association with the sharp endothermic peak denoted as IV in Fig.3a. During this stage, the evolved gases still consist of CO_2 and 6-undecanone, but the absorbance of the later relative to that of CO_2 has doubled in comparison to stage III (358°C in Fig.7). Simultaneously, the FTIR spectra of the solid residues show that the absorption bands due to the hexanoate ligands progressively disappear (Fig.5). For example, the CH_2 and CH_3 stretching bands between 2800 cm^{-1} and 3000 cm^{-1} are just hardly visible in the sample quenched from 450°C, while the features appearing between 800 cm^{-1} and 1650 cm^{-1} are typical for an oxycarbonate [44]. The formation of such a compound is confirmed by the in-situ XRD patterns (Fig.6b) showing the appearance of a new set of diffraction peaks around 368°C. The ICDD PDF-2 database (2013 release) does not contain reference patterns for Ce-oxycarbonates, but the close analogy between the position and relative intensity of the observed peak with the reference data for the hexagonal form of $La_2O_2CO_3$ (ICDD card number 37-804) allows attributing the new diffraction pattern to a $Ce_2O_2CO_3$ dioxymonocarbonate compound that becomes clearly visible from 388°C and has its strongest intensity between 408°C and 469°C. In contrast, the low angle diffraction peak that formed during stage III vanishes during heating above 378°C (Fig.6a). These transformations indicate that the sample undergoes a decomposition corresponding to:

$$Ce_2O(C_5H_{11}CO_2)_4 \rightarrow Ce_2O_2CO_3 + 2C_5H_{11}COC_5H_{11} \nearrow + CO_2 \nearrow \qquad (2)$$

The expected overall mass loss relative to the $Ce(C_5H_{11}CO_2)_3$ starting composition is 61.6%. The experimental FTIR data show that the reaction is complete between 450°C and 460°C,

corresponding to 59.1 % ≤ Δm ≤ 60.1 %. This observed mass loss is a little too low and this will be discussed in relation to the last decomposition process.

Above 460°C, the sample's mass slowly decreases and reaches a constant value at approximately 720°C, where the total mass loss is 64.0 % and compares well with 64.5 % for a final decomposition into CeO_2. The formation of the latter compound is confirmed by the in-situ XRD patterns (Fig.6b, 555°C). This means that Ce^{3+}, which was present in the starting $Ce(C_5H_{11}CO_2)_3$ and all the way to $Ce_2O_2CO_3$, has increased its valency to Ce^{4+}. The question arises as when this event took place. A close inspection of the XRD patterns (Fig.6b) from 439°C to 498°C reveals the presence of a peak at $2\theta = 2.42°$ that can be attributed neither to $Ce_2O_2CO_3$ nor to CeO_2. Instead, it could correspond to the highest intensity reflection of Ce_2O_3 (ICDD card number 78-484, (011) reflection with d = 2.945 Å). This indicates that $Ce_2O_2CO_3$ first decomposes to Ce_2O_3 which is then rapidly oxidized to CeO_2. Since the decomposition of $Ce_2O_2CO_3$ into Ce_2O_3 is accompanied by the evolution of CO_2 as shown by the evolved gas FTIR spectra at 455°C and 632°C in Fig.7, we assume that the oxygen source responsible for the Ce_2O_3 to CeO_2 transformation is the residual O_2 present in the Ar carrier gas (<0.5 ppm). In this way, the last reaction steps would be as follows:

$$Ce_2O_2CO_3 \rightarrow Ce_2O_3 + CO_2 \nearrow \qquad (3)$$

$$Ce_2O_3 + ½\ O_2 \rightarrow 2CeO_2 \qquad (4)$$

The oxidation reaction (4) is expected to be exothermic. An exothermic contribution to the DTA trace can indeed be distinguished in Fig. 3a starting at approximately 450°C. The temperature at which this reaction ends is difficult to determine on the DTA trace but it is likely that it proceeds until the end of the overall thermal decomposition process. As evidenced in the DTA and TG traces, reactions (1) to (4) partly overlap each other, most probably as a result of the limited thermal stability of the various intermediate products. If reaction (4) starts to some extent before full

completion of reaction (2), the input of oxygen in the solid residue during the Ce^{3+} - Ce^{4+} transformation will contribute with a net mass increase of the sample, superimposed on the mass loss resulting from reactions (2) and (3). In this way, the mass loss value observed at 460°C (60.1%) will be evidently lower than theoretically expected for the formation of $Ce_2O_2CO_3$ as mentioned above. Interestingly, the macroscopic morphology of the solid residue does not vary significantly during reactions (2), (3) and (4) besides an overall shrinkage that can be observed by comparing the optical micrographs taken at 320°C and 600°C (Fig.4).

3.2 Ce pentanoate

The FTIR spectrum of the as synthesized Ce-pentanoate sample is presented in Fig. 1. It contains all the specific absorption bands of a rare-earth pentanoate salt [45]. Like in the case of Ce-hexanoate, the characteristic absorption bands of the starting reagent Ce-acetate at 1017 cm^{-1} and 1054 cm^{-1} are not visible, whereas the strong absorption band from the COOH group of pentanoic acid at 1712 cm^{-1} is absent [37], showing that the solvent has been evaporated. The $\Delta\nu$(COO) value is of 128 cm^{-1}, i.e. close to that of Ce-hexanoate, suggesting a similar coordination type. This dried Ce-pentanoate salt ($Ce(C_4H_9CO_2)_3$) appears to be poorly crystallized and does not give rise to a well-defined XRD pattern. Instead, only a broad diffraction peak appears around $2\theta = 0.52°$, like for the in-situ pattern recorded at 78°C shown in Fig.S1.

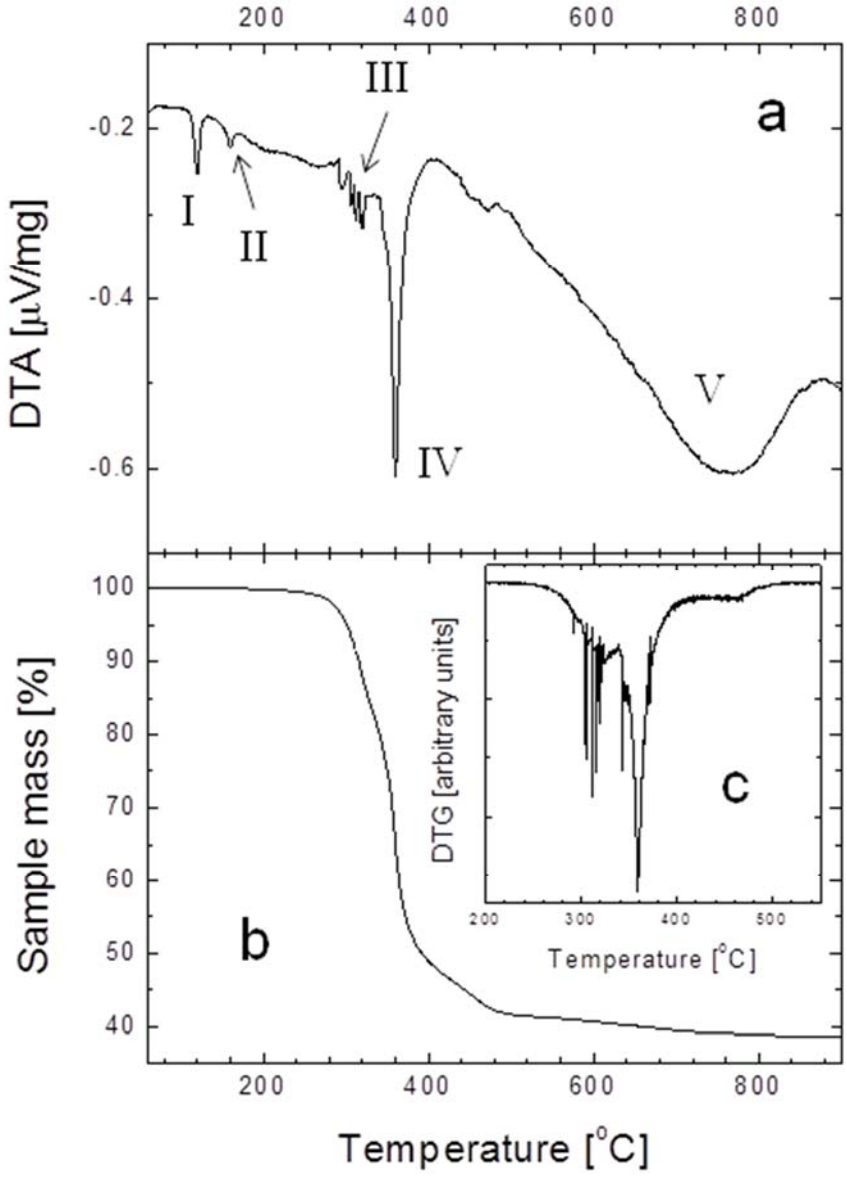

Figure 8: DTA (a), TG (b) and DTG (c) traces recorded on Ce-pentanoate upon heating at 5°C/min in Ar.

The DTA, TG and DTG traces obtained during heating the Ce-pentanoate powder in Ar flow at 5 °C/min are shown in Fig 8 a, b and c respectively. The observed features are quite similar to those appearing for Ce-hexanoate. There are again two endothermic peaks at T < 200°C. The first has an onset at 109°C and extremum at 120°C. The FTIR spectrum of the sample after quenching

from 135°C is unchanged in comparison to the virgin sample (Fig.S2) and the in-situ XRD pattern only shows a decrease of the intensity of the single broad scattering peak at 2θ = 0.52° (Fig. S1, patterns at 78°C and 143°C). This indicates that the pentanoate molecular structure is not affected by this first endothermic event and that only the short range crystallographic coherence is disturbed to some extent. These characteristics suggest a phase transition similar to that discussed in the previous section for the Ce-hexanoate crystalline – liquid crystalline phase transformation, although this cannot directly be confirmed by X-ray diffraction due to the lack of crystallinity of the compound. The hot stage optical micrographs do not show significant changes before and after this peak (Fig.S3, 65°C and 130°C), besides a slight change of color and the appearance of shiny light reflections on some of the powder particles. This behavior is somehow similar to that observed in the Ce-hexanoate powders in the same temperature range (Fig.4). The second endothermic peak (II in Fig 8a), has an onset near 145°C and minimum at 160°C. Again, no significant changes are seen in the FTIR spectrum of a sample quenched from 195°C (Fig.S2), while the intensity of the broad diffraction peak in the XRD patterns only appears to decrease further (Fig.S1, 200°C and 284°C). The in-situ optical image recorded at 170°C shows that the particles have become translucent (Fig.S3). While this is indicating that the endothermic stage II is related to a melting process, the viscosity of the molten phase is clearly much higher than after the stage II transition to isotropic liquid observed in Ce-hexanoate as the Ce-pentanoate particles are still held together instead of coalescing and spreading over the sample holder.

Upon further heating, the sample mass starts decreasing significantly above 260°C, while the DTA and DTG traces have a stochastic behavior superimposed on an endothermic peak (Fig.8 b and c). This stage III is followed by a sharp endothermic peak (IV in Fig.8a) with onset at 343°C. This sequence of events is similar to that of events III and IV discussed above for Ce-hexanoate.

However, the TG trace of Ce-pentanoate in this range presents a more marked kink with acceleration of the mass loss rate during stage IV. The increase of the separation of stages III and IV is also evidenced in the DTG trace that shows a better resolved double-peak structure (Fig.8c). The optical micrographs show that stage III includes a solidification of the sample (320°C in Fig.S3). At the same time, the Δν(COO) difference calculated using the FTIR spectra of quenched samples decreases (128 cm^{-1} at 195°C versus 122 cm^{-1} at 330°C). The mass loss at 343°C, i.e. just before the onset of the DTA endothermic peak IV and in correspondence with the kink in the TG trace is equal to 21.2%, in close agreement with the 21.0% theoretically expected for the formation of a $Ce_2O(C_4H_9CO_2)_4$ intermediate product. During stage III, CO_2 and $C_4H_9COC_4H_9$ (5-nonanone) are evolving from the sample as shown in Fig.S4 (319°C). These features allow proposing that stage III is closely related to stage III for Ce-hexanoate so that equation (1) can be generalized as:

$$2Ce(C_nH_{2n+1}CO_2)_3 \rightarrow Ce_2O(C_nH_{2n+1}CO_2)_4 + C_nH_{2n+1}COC_nH_{2n+1} \nearrow + CO_2 \nearrow \qquad (5)$$

with n = 5 and 4 for Ce-hexanoate and Ce-pentanoate respectively.

By the end of stage III, the broad low angle XRD peak has moved to a lower 2θ position (Fig.S1, 341°C) and two peaks develop in this scattering range with maximum intensity at 375°C prior to disappearing again around 390°C, i.e. simultaneously with the end of the DTA peak IV. In the high 2θ range (Fig.S5), a peak that cannot be attributed to $Ce_2O_2CO_3$, Ce_2O_3 or CeO_2 also has a maximum intensity at 375°C and disappears upon further heating. It is not impossible that these short-lived XRD peaks belong to the $Ce_2O(C_4H_9CO_2)_4$ intermediate phase.

During stage IV, the same gas species are released from the sample as during reaction (5), with a doubling of the relative intensity of 5-nonanone relative to that of CO_2 (Fig.S4, 361°C) and the FTIR spectra of quenched samples demonstrate the collapse of the pentanoate ligands (Fig.S2 400°C – 420°C). The last traces of CH_2 and CH_3 stretching vibrations between 2850 cm^{-1} and 3000

cm^{-1} disappear near 420°C. At 420°C, the overall mass loss amounts to 53.1%. This is quite smaller than the 58.0% expected for the formation of $Ce_2O_2CO_3$, which is expected from the FTIR spectrum left after quenching from 420°C as well as the in-situ XRD patterns showing the presence of this compound at 414°C to at least 480°C (Fig.S5). Since the final decomposition product is CeO_2, this discrepancy in mass loss values could possibly also be related to the uptake of some oxygen considering that $Ce_2O_2CO_3$ is unstable and probably starts decomposing very soon after its formation. We therefore propose that the main reaction taking place during stage IV is similar to stage IV in Ce-hexanoate so that equation (2) can be generalized as (n = 5 or 4):

$$Ce_2O(C_nH_{2n+1}CO_2)_4 \rightarrow Ce_2O_2CO_3 + 2C_nH_{2n+1}COC_nH_{2n+1} \nearrow + CO_2 \nearrow \quad (6)$$

It must nevertheless be mentioned that the formation of $Ce_2O(CO_3)_2$ instead of $Ce_2O_2CO_3$ would result in a mass loss of 51.5%, i.e. the observed Δm value is in between those expected for the formation of each of these two different oxicarbonate phases. This point will be discussed in more detail in the next two sections.

Above 420°C, the sample mass continues decreasing at a slower rate with release of CO_2 (Fig.S4: 492°C and 644°C) and becomes constant at 850°C (Fig.8b). At that point, the total experimental mass loss reaches 61.4% in excellent agreement with the 61.2% that are theoretically expected for the overall decomposition of $Ce(C_4H_9CO_2)_3$ into CeO_2. The XRD patterns actually confirm that this end compound is being formed in the sample (533°C in Fig.S5). Like in the case of Ce-hexanoate, the transient presence of Ce_2O_3 is hinted at in the in-situ XRD patterns by some diffraction intensity at $2\theta = 2.42°$, although this is less evident in the case of Ce-pentanoate (Fig.S5: 414°C to 502°C). This leads to the suggestion that the last stages of Ce-pentanoate decomposition can be described by equations (3) and (4):

An exothermic feature appears in the DTA trace between 460°C and 520°C on top of the broad endothermic peak related to the decomposition of the Ce-oxycarbonate (Fig. 8a). While the Ce^{3+} to Ce^{4+} transition might be involved in this feature, it is more prominent than in the case of Ce-hexanoate and might as well be due at least in part to the burning of some residual carbonaceous residue that may result from side reactions during the pyrolysis of Ce-pentanoate, 5-nonanone or of the oxycarbonate as mentioned for example in relation to the thermal decomposition of Y-pentanoate [45]. This would fit with the strong color change taking place between 410°C and 530°C observed by in-situ optical microscopy (Fig.S3).

3.3 Ce butanoate

The FTIR spectrum of the as-prepared Ce-butanoate sample is plotted in Fig.1. It contains all the absorption bands characteristic for a rare-earth butanoate [46,47]. In contrast to Ce-pentanoate and Ce-hexanoate, the presence of O-H vibrations is evidenced among others by the broad absorption between 3100 cm^{-1} and 3600 cm^{-1}. The DTA, TG and DTG traces obtained from this sample are shown in Fig.9 a-c. A first endothermic peak (I in Fig.9a) developing from 60°C to 120°C, is accompanied by a mass loss of 4.5% that would correspond to the loss of one mole of H_2O per mole of $Ce(C_3H_7CO_2)_3$ (theoretical mass loss = 4.3%). The release of H_2O is evidenced in the FTIR spectrum recorded at 93°C on the evolved gas (Fig.S6) and further confirmed by the FTIR spectrum of a sample quenched from 150°C in which the O-H vibration absorption bands are no longer visible (Fig.S7). The hot-stage optical micrographs taken at 50°C and 130°C (Fig.S8) show hardly any difference. However, the XRD patterns clearly show that changes are taking place in the structure (Fig.S9). Up to 94°C, no changes are noticed, but at 129°C, new diffraction peaks have replaced the original pattern, with the highest intensity peak at a 2θ angle higher than for the starting salt. This is akin to what was observed in Ce-hexanoate in relation to the first endothermic

peak appearing in this compound, the main difference being that the relative peak positions are shifted to higher 2θ angles for Ce-butanoate as can be expected from the shorter alkanoate chain. An essential difference however, is that there was no H_2O loss in Ce-hexanoate. Since the modification of the XRD pattern only take place above 94°C, i.e. more than 30°C above the onset of the H_2O release, it can be inferred that a structural transition independent of the dehydration process is taking place. A structure can indeed be seen in the DTA trace on the high temperature side of DTA peak I as shown in the inset of Fig. 9a. Dehydration does not seem to result in changes in the XRD pattern, as the pattern recorded at 109°C (Fig.S9) shows a superposition of the starting peaks and those present at 129°C. In rare-earth alkanoates, water molecules normally situated in the ionic layers and do not influence the lamellar structure, whence dehydration would not induce significant changes in the XRD patterns [40].

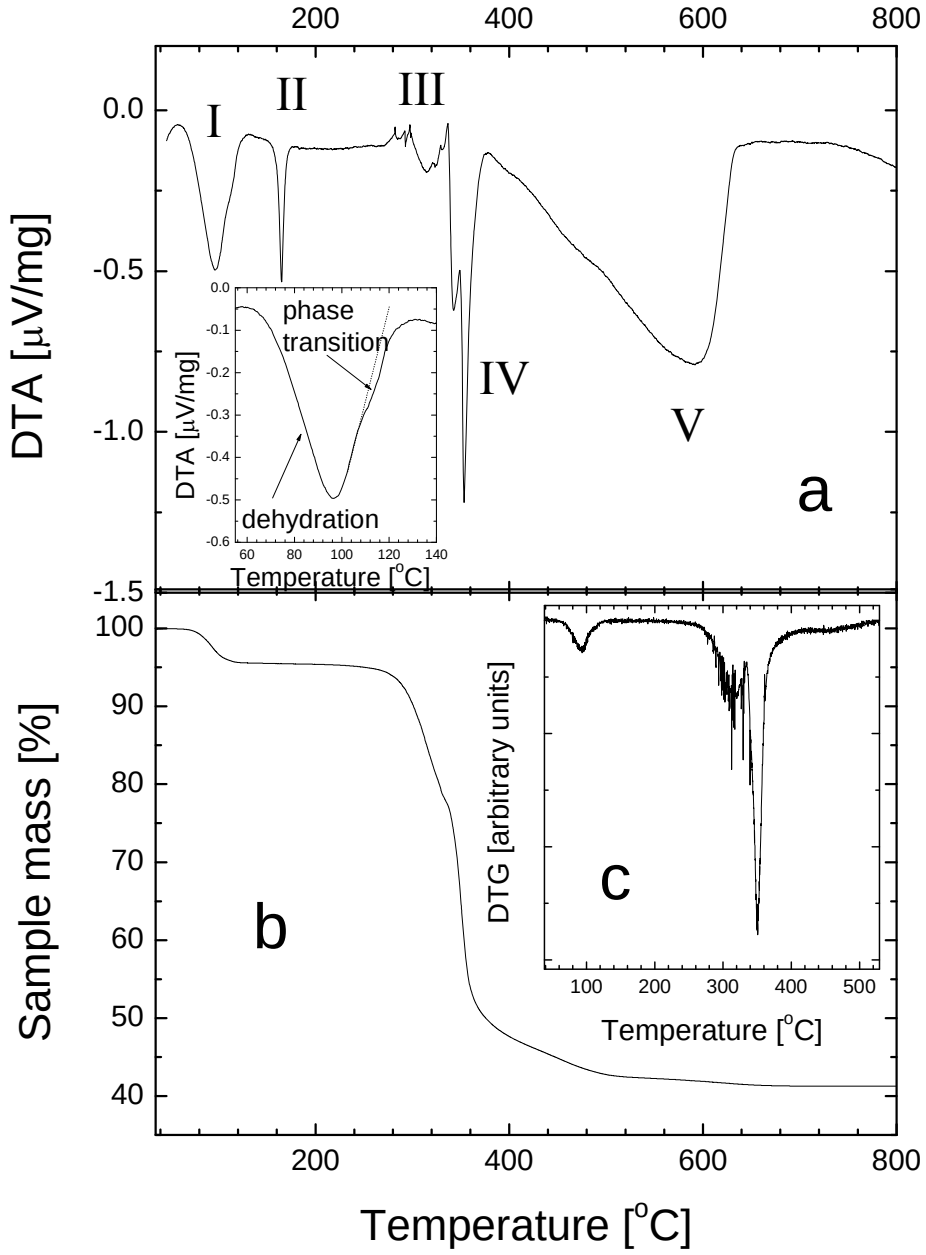

Figure 9: DTA (a), TG (b) and DTG (c) traces recorded on Ce-butanoate monohydrate upon heating at 5°C/min in Ar. Inset in (a): detail of the DTA trace at low temperature.

The next endothermic peak (II in Fig.9a) is accompanied by the collapse of the XRD peaks as shown in Fig.S9, where only a broad diffraction peak is left around 2θ = 0.58° at 188°C. The butanoate molecular arrangement survives this endothermic reaction as shown by the FTIR

spectrum of the sample quenched from 200°C (Fig.S7). It is thus tempting to attribute the reaction labelled as II to a transition to an isotropic liquid state. Nevertheless, the hot-stage microscope image at 180°C (Fig.S8) does not show evidence for extended melting. It is therefore more likely that the sample undergoes a crystalline solid – amorphous solid transition resulting in an amorphisation of this structure, unless a liquid with very high viscosity has formed.

Further heating brings about a broad endothermic peak (III in Fig.9a) with superimposed exothermic features. While this situation is similar to that observed in Ce-pentanoate, endothermic peak III is now much better separated from the sharp endothermic peak developing at higher temperature. The TG trace (Fig.9b) also exhibits a step that reminds the kink seen for Ce-valerate in the same temperature range. Analysis of the gas evolved during this stage III (317°C in Fig.S6) demonstrates the release of CO_2 and $C_3H_7COC_3H_7$ (4-heptanone). With a mass loss of 22.8% at the end of endothermic peak III (337°C), which corresponds very well with the 23.1% expected for the decomposition of $Ce(C_3H_7CO_2)_3 \cdot H_2O$ to $Ce_2O(C_3H_7CO_2)_4$, the first stages of decomposition of the compound studied in this section can be described as dehydration followed by reaction (5) with n = 3.

Similarly to the observations made for Ce-hexanoate and Ce-pentanoate, it was found that $\Delta\nu$(COO) decreases during reaction (8) from 136 cm^{-1} to 124 cm^{-1} (at 330°C, cf Fig.S7). Concerning the XRD patterns, during stage III, the low 2θ range shows that the low intensity, broad peak shifts from 0.58° to 0.50° (222°C to 349°C in Fig.S9) in a fashion similar to what was happening in Ce-pentanoate during the same decomposition stage. It can be noted that stage III results in severe shrinkage of the powder as evidenced in Fig.S8 (300°C).

The next stage, labelled IV in Fig.9a, is more complicated than for Ce-hexanoate and Ce-pentanoate, because the sharp endothermic peak is now showing evidence for 2 overlapping

reactions. Due to the fast kinetics of these reactions as reflected by both the steepness of the TG trace in this temperature range and the narrow width of the overlapping endothermic peaks, it is not possible to distinguish evident features in the DTG trace. The gas species evolving from the sample during the first half of stage IV still consist of CO_2 and 4-heptanone (Fig.S6 345°C). However, contrary to what was observed during the stage IV of Ce-hexanoate and Ce-pentanoate, the intensity ratio of the absorption bands of these two compounds is not changed. This could fit with a decomposition scheme given by:

$$Ce_2O(C_3H_7CO_2)_4 \rightarrow 2CeO(C_3H_7CO_2) + C_3H_7COC_3H_7 \nearrow + CO_2 \nearrow \qquad (7)$$

which does not require a doubling of the amount of 4-heptanone relative to CO_2 like in the case of reactions (2) and (6) and would agree with the FTIR spectrum of the quenched solid residues (Fig.S7), which show that the alkanoate ligands are still detectable up to 375°C. Though, the mass loss at the temperature corresponding to the local positive maximum between the double DTA peak (349°C), which is equivalent to 33.4% is quite far away from the 42.0% expected for the formation of $2CeO(C_3H_7CO_2)$ from the starting $Ce(C_3H_7CO_2)_3 \cdot H_2O$ so that the formation of this intermediate compound is highly conjectural.

A clearer conclusion can be drawn upon the completion of the second endothermic contribution of the overlapping stage IV. At the end of that composite feature, i.e. 378±2°C, the mass loss amounts to 50.3%, which is close to the value expected for the formation of $Ce_2O(CO_3)_2$ (50.4%). The presence of this oxycarbonate phase is confirmed by the in-situ XRD patterns, where peaks that can be attributed to it by analogy with the reference pattern for $La_2O(CO_3)_2$ (ICDD card number 41-672), emerge from the background at 365°C and increase in intensity up to 399°C before progressively disappearing again (Fig.S10). The last traces of butanoate ligands are found to disappear from the FTIR spectra of the quenched samples between 375°C and 385°C (Fig.S7),

in agreement with the formation of the oxycarbonate, which would thus be following the reaction (assuming reaction (7) above):

$$Ce_2O_2(C_3H_7CO_2)_2 \rightarrow Ce_2O(CO_3)_2 + C_3H_7COC_3H_7 \nearrow \quad (8)$$

Or possibly $$Ce_2O(C_3H_7CO_2)_4 \rightarrow Ce_2O(CO_3)_2 + 2C_3H_7COC_3H_7 \nearrow \quad (9)$$

These two reactions involve no CO_2 evolution. While the FTIR spectrum of the evoved gas shows a surge of $C_3H_7COC_3H_7$ during stage IV (352°C in Fig.S6), CO_2 is still observed. However, each spectrum in Fig.S6 is an average over several scans and includes the gas species entering the gas cell over 1 minute for a 5°C/min heating ramp. Furthermore, the gas cell probed by the laser of the FTIR spectrometer is not immediately flushed by the newly incoming gas so that we can estimate that those spectra not only still contain some CO_2 released during the end of stage III or reaction (7), while CO_2 could possibly already start to evolve from the decomposition of unstable $Ce_2O(CO_3)_2$. Due to these limitations in the time resolution of evolved gas FTIR analysis, it is preferable to rely on the evidence provided by the in-situ patterns that strongly support the conclusion that $Ce_2O(CO_3)_2$ has formed and thereby that at least one of reactions (8) and (9) takes place during stage IV.

Above 390°C, only CO_2 evolution is detected by FTIR (Fig. S6, 451°C and 582°C). This occurs in parallel with the progressive transformation of $Ce_2O(CO_3)_2$ to $Ce_2O_2CO_3$ and finally CeO_2 as revealed by the in-situ XRD patterns (Fig.S10, 399°C to 530°C). Like for Ce-hexanoate and Ce-pentanoate, the transient presence of Ce_2O_3 is hinted at by the XRD peak visible at 2.42° in Fig.S10 (mostly discernable at 410°C). The last stages of Ce-butanoate decomposition in Ar can therefore be described as $Ce_2O(CO_3)_2 \rightarrow Ce_2O_2CO_3 + CO_2 \nearrow$ followed by reactions (3) and (4). With a total mass loss of 59.0 %, which is very close to the 58.9% theoretically expected for the decomposition of $Ce(C_3H_7CO_2)_3 \cdot H_2O$ into CeO_2.

3.4 Discussion

Besides dehydration in Ce-butanoate, Ce-hexanoate, pentanoate and butanoate all exhibit two transitions below 200°C, during which their molecular integrity is preserved. The nature of the first transition was not studied in details but is most probably of a solid to liquid crystal nature, based on the observation of partial melting in at least Ce-pentanoate and Ce-hexanoate as well as the appearance of a new diffraction pattern in the in-situ XRD studies for Ce-butanoate and Ce-hexanoate. The second endothermic transition is always accompanied by the loss of long range ordering, although this is less evident for Ce-pentanoate that was poorly crystallised. The temperatures at which the related endothermic DTA peaks have their maximum intensity are reported in Table 1. There is a clear tendency for a temperature increase for both features when the alkanoate chain length decreases. This fits well with the data presented in [40] and continues the trend observed for the Ce-hexanoate to Ce-decanoate salts for the mesophase – smectic A and smectic A – isotropic liquid transitions. Brzyska and Paszkowska [30] did not observe these transitions in Ce-hexanoate, maybe merely due to the large dehydration DTA peak that spreads over a large temperature span owing to the faster heating rate (10°C/min) used in their study. The DTA traces published for the thermal decomposition of Ce-pentanoate monohydrate in air and N_2 by Lazareva et al. [29] exhibit a double endothermic peak between 90°C and 150°C. The first contribution is certainly due to dehydration, but the second, which is not discussed in [29], is most probably related to the transition to isotropic liquid state. The occurrence of melting transitions is a common feature in rare earth alkanoates with ligands containing 4 to 6 carbon atoms. This had already been reported in hexanoates of La, Ce, Pr, Nd and Y [35,36,40,48-50], La, Nd and Y pentanoates [36,45,48,50] as well as La, Nd, Er, Tm, Yb, Lu and Y butanoates [46-48,50,51].

Figure 10 compares the DTA traces of Ce-butanoate, Ce-pentanoate and Ce-hexanoate between 190°C and 410°C. This temperature interval comprises the signature of recrystallization in the form of exothermic spikes superimposed on a broad endothermic peak related to the first stage of decomposition. If the decomposition taking place during stage III (reaction (5)) proceeds from the surface of the molten compounds and is followed by the formation of a solid surface layer consisting of the reaction product $Ce_2O(C_nH_{2n+1}CO_2)_4$ with n = 3, 4, 5 for Ce-butanoate, pentanoate an hexanoate respectively, the further decomposition inside the internal volume that is still molten can be slightly delayed due to the formation of an internal overpressure of decomposition gases. However, as the internal pressure increases beyond some limit the solid crust will be broken and molten Ce-butanoate, pentanoate or hexanoate will be exposed to conditions favoring their decomposition. This mechanism could explain the occurrence of several exothermic spikes along the DTA trace during stage III as well as the sudden surges of mass loss evidenced by the irregular DTG curves in the corresponding temperature intervals. The stochastic nature of these irregular features in the DTA and DTG traces is confirmed by the fact that their detail structure is not reproducible from one run to another on samples from the same batch. A similar characteristic behavior has been already reported for several rare-earth alkanoates that undergo melting prior to decomposition [35,36,45-47].

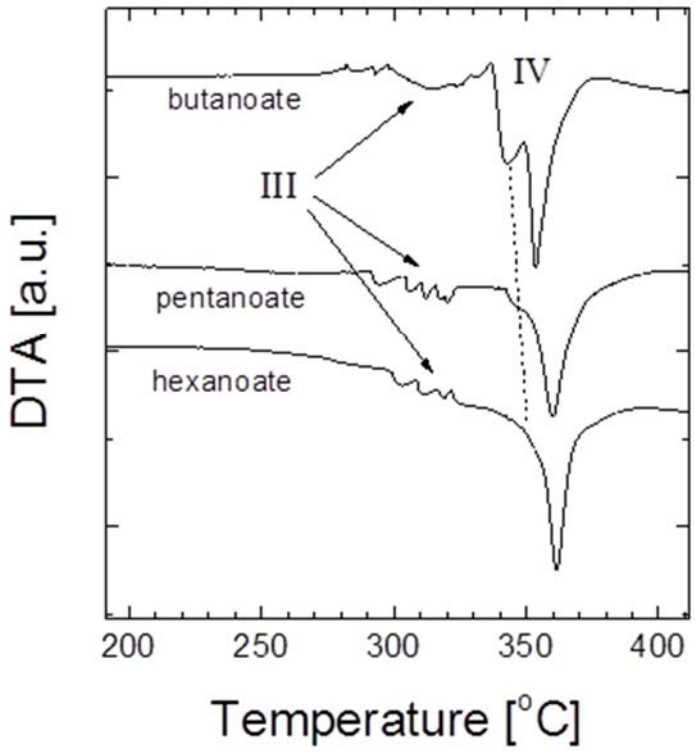

Figure 10: Comparison of the DTA traces of Ce-butanoate monohydrate, Ce-pentanoate and Ce-hexanoate between 190°C and 410°C.

The previously published DTA trace of Ce-hexanoate decomposition [30] was measured in air and additional exothermic effects due to burning of organic moieties naturally prevent the detection of such effects. Huge exothermic DTA peaks are also present during the thermal decomposition of Ce-pentanoate in [29], not only in air, but in N_2 as well, which is surprising.

Figure 10 also shows the sharp endothermic peak structure (IV) leading to the formation of the cerium oxycarbonate. Besides a lowering of the temperature at which this event takes place as also shown in Table 1, it is evident that peak IV transforms from a single peak to a double peak when the ligand chain length decreases. Studies on the thermal decomposition of Ce-acetate by Arii et al. [24,25] also resolved a two-peak structure in this area and concluded to a three step

decomposition reaction (including the first event labelled III in the present work) that involves steps equivalent to reactions (5), (7) and (8) with n = 1:

On the other hand, the DTA trace for the decomposition of Ce-propanoate published by Ogawa [26] also shows a multi-peak structure, but the author only mention a $Ce_2O(C_2H_5CO_2)_4$ intermediate product.

As exposed in the previous sections, the occurrence of a $Ce_2O(C_nH_{2n+1}CO_2)_4$ stage can be established for Ce-butanoate (n = 3), Ce-pentanoate (n = 4) and Ce-hexanoate (n = 5) based on TG data, but the $Ce_2O_2(C_nH_{2n+1}CO_2)_2$ intermediate could only be hypothesized for Ce-butanoate. However, if the low temperature part of the double endothermic structure IV actually corresponds to the formation of such a compound as could be expected by analogy with the decomposition of Ce-acetate [24,25], it is most likely that the low temperature shoulder on peak IV for Ce-pentanoate is due to the same type of reaction but with an even lower stability of an hypothetical $Ce_2O_2(C_4H_9CO_2)_2$ intermediate product. Whether a $Ce_2O_2(C_5H_{11}CO_2)_2$ intermediate forms during the decomposition of Ce-hexanoate or not is not clear and an answer to this question would require further specific investigations. The fact that oxo-alkanoate intermediate phases form during the decomposition of rare-earth alkanoates and are less and less stable as the ligand chain length increase has already be observed for Y and La alkanoates [35,36,45-47] and is certainly a common feature of this type of compounds. In any case, the observation of these intermediates requires a high enough resolution and a relatively slow heating rate. The use of an oxidizing atmosphere that increases the local temperature due to burning processes and thereby accelerates the reaction rates is also a major obstacle. These reasons probably contribute to the fact that oxo-alkanoate intermediates were not reported in previous studies on Ce-butanoate, pentanoate and hexanoate thermal decomposition [28-30].

The final decomposition product is CeO_2 in all cases and proceeds via at least one oxycarbonate phase: $Ce_2O_2CO_3$. The possible observation of an additional transient $Ce_2O(CO_3)_2$ phase in the course of Ce-butanoate thermal decomposition would be in line with the apparent increasing complexity of the decomposition behavior of the cerium alkanoates with decreasing ligand chain length. The occurrence of cerium oxycarbonates has been rarely reported in relation with thermal decomposition studies of cerium carboxylates, for instance in the case of Ce-propionate, formate, acetate ($Ce_2O_2CO_3$ only) [22,25,26] or Ce-oxalate $Ce_2O(CO_3)_2$ [52]. However, a direct decomposition from the metalorganic framework to CeO_2 without oxycarbonate intermediate is generally reported e.g. [53-62]. Nevertheless, in those last instances, the absence of an oxycarbonate stage was systematically inferred from the absence of a constant mass plateau in the TG traces. It is not impossible that FTIR measurements of quenched samples would also reveal an oxycarbonate stage if the thermal stability of such compounds is limited, especially when air is used as a carrier gas during the measurements as was the case for references [53-62].

Conclusions

The thermal behavior and decomposition of Ce-butanoate monohydrate ($Ce(C_3H_7CO_2)_3 \cdot H_2O$), Ce-pentanoate ($Ce(C_4H_9CO_2)_3$) and Ce-hexanoate ($Ce(C_5H_{11}CO_2)_3$) in argon atmosphere is a complex process, which seems to become more complicated as the ligand chain length decreases. Dehydration of $Ce(C_3H_7CO_2)_3 \cdot H_2O$ starts around 60°C. The fact that the other two compounds were obtained in an anhydrous state is probably only due to the temperature (60°C) used for evaporating the solvent during sample synthesis.

Before decomposition, all three compounds undergo two transitions, seemingly related to the formation of a liquid crystalline state followed by melting to an isotropic liquid, although the viscosity of the melts for Ce-butanoate and Ce-pentanoate appears to be rather high.

During the first stage of decomposition, a mixed oxo-alkanoate compound was evidenced in all three salts via a reaction of the type:

$$2Ce(C_nH_{2n+1}CO_2)_3 \rightarrow Ce_2O(C_nH_{2n+1}CO_2)_4 + C_nH_{2n+1}COC_nH_{2n+1} \nearrow + CO_2 \nearrow$$

with n=3 (Ce butanoate), n=4 (Ce-pentanoate) and n=5 (Ce-hexanoate).

The end decomposition product consists of CeO_2. The formation of the $Ce_2O_2CO_3$ oxycarbonate intermediate was observed for all compounds. However, the possible occurrence of additional intermediates such as $Ce_2O_2(C_nH_{2n+1}CO_2)_2$ and $Ce_2O(CO_3)_2$ between the $Ce_2O(C_nH_{2n+1}CO_2)_4$ and $Ce_2O_2CO_3$ stages becomes more and more obvious as the ligand chain length decreases. This trend appears to be in line with previous studies dealing with the thermal decomposition of Ce-acetate. Nevertheless, the formation of $Ce_2O_2(C_3H_7CO_2)_2$ in the course of Ce-butanoate decomposition could not be unambiguously confirmed. This may be due to the very low thermal stability of this compound and more investigations using techniques with higher time resolution will be necessary to confirm its occurrence.

The observation of an XRD peak belonging to Ce_2O_3 suggests that oxidation of Ce from trivalent to tetravalent state takes place after the decomposition of the oxycarbonate phase. The occurrence of strongly reducing agents such as ketones among the gaseous decomposition products released during the thermal decomposition of Ce-alkanoates certainly plays a role in stabilizing Ce^{3+} and thereby $Ce_2O_2CO_3$ in spite of the residual oxygen present in the carrier gas. However, at 450°C, the release of ketones is essentially finished so that conditions are favorable for the conversion of Ce^{3+} to Ce^{4+}. In air, the situation would be different and Ce_2O_3 as well as even $Ce_2O_2CO_3$ may not appear at all as intermediate species.

The fact that the thermal decomposition of these compounds takes place via several stages as well as their properties of melting to various extents prior to decomposing, means that several heat

treatment parameters are potentially available in order to manipulate the morphology of the final CeO_2 powders as well maybe as that of the $Ce_2O_2CO_3$ intermediate phase particles in view of specific applications.

Besides CO_2, the decomposition results in the release of symmetrical ketones, i.e. 4-heptanone, 5-nonanone or 6-undecanone for Ce-butanoate, Ce-pentanoate and Ce-hexanoate respectively. These substances are classified as toxic by inhalation, ingestion and skin contact, although they are not highly dangerous. Mass production of ceria nanoparticles by means of thermal decomposition would therefore require further decomposition of these educts by combustion, although they may as well as be condensed in view of use as valuable chemicals as solvents, food grade flavor ingredient (4-heptanone), supported liquid membrane (6-undecanone), etc.

The decomposition of Ce-butanoate, pentanoate and hexanoate was here determined in argon. Heating in air flow is likely to result in partial combustion of the symmetrical ketones with formation of H_2O and additional CO_2 accompanied by strong exothermic effects. This will also contribute to the destabilization of some intermediate products. Knowledge of the extent of such reactions requires further studies based on relevant processing parameters including P_{O2}, atmosphere humidity, heating rate, gas flow, etc.

Acknowledgements

This work was supported by the Danish Agency for Science, Technology and Innovation under contract nr. 09-062997 and by DTU project nr. 49605-E5. The authors also acknowledge financial support from DANSCATT as well as DESY/HASYLAB (project I-20110113 EC). These funding sources have no role in study design; in the collection, analysis and interpretation of data; in the writing of the report; and in the decision to submit the article for publication.

References

[1] Singh S., Cerium oxide based nanozymes: Redox phenomenon at biointerfaces, Biointerphases 11 (2016) 04B202

[2] Zhang Y., Wei W., Das G.K. and Tan T.T.Y., Engineering lanthanide-based materials for nanomedicine, J. Photochemistry and Photobiology C: Photochemistry Reviews 20 (2014) 71 - 96

[3] Kyosseva S.V. and McGinnis J.F., Cerium oxide nanoparticles as promising ophthalmic therapeutics for the treatment of retinal disease, World J. Ophthalmol. 5 (2015) 23 – 30

[4] Bsat S., Speirs A. and Huang X., Recent trends in newly developed plasma-sprayed and sintered coatings for implant applications, J. Thermal Spray Technology 25 (2016) 1088 – 1110

[5] Nelson B.C., Johnson M.E., Walker M.L., Riley K.R. and Sims C.M., Antioxidant cerium oxide nanoparticles in biology and medicine, Antioxidants 5 (2016) 15

[6] Diaconeasa Z., Barbu-Tudoran L., Coman C., Leopold L., Mesaros A., Pop O., Rugina D., Stefan R., Tabaran F., Tripon S. and Socaiu C., Cerium oxide nanoparticles and its cytotoxicity human cancer cells, Romanian Biotechnological Letters 20 (2015) 10679 - 10687

[7] Boyjoo Y., Su H.Q., Liu J., Pareek V.K. and Wang S.B., A review on photocatalysis for air treatment: From catalyst development to reactor design, Chem. Eng. J. 310 (2017) 537 - 559

[8] Bineli A.R.R., Tasic M.B. and Maciel R, Catalytic steam reforming of ethanol for hydrogen production: brief status, Chemical Industry & Chemical Engineering Quarterly, 22 (2016) 327 – 332

[9] Barbato P.S., Di Benedetto A., Landi G. and Lisi L., Structuring CuO/CeO_2 catalyst as option to improve performance towards CO-PROX, Top. Catal. 59 (2016) 1371 – 1382

[10] Tumuluri U., Rother G. and Wu Z.L., Fundamental understanding of the interaction of acid gases with CeO_2: From surface science to practical catalysis, Industrial & Engineering Chemistry Research 55 (2016) 3909 - 3919

[11] Montini T., Malchionna M., Monai M. and Fornasiero P., Fundamentals and catalytic applications of CeO_2-based materials, Chem. Rev. 116 (2016) 5987 – 6041

[12] Wang H., Cao L.Y., Wang Y., Jin L.H., Lu J.F., Li C.S. and Huang J.F., Effect of lattice mismatch between substrate and CeO_2 on the epitaxial growth of CeO_2 buffer layer, Rare Metal Materials and Engineering 44 (2015) 2250 – 2254

[13] Lu Y.M., Cai S., Liang Y., Bai C.Y., Liu Z.Y., Guo Y.Q. and Cai C.B., The mechanism of the nano-CeO_2 films deposition by electrochemistry method as coated conductor buffer layers, Physica C 512 (2015) 1 - 5

[14] Hosokawa S., Synthesis of metal oxides with improved performance using a solvothermal method, J. Ceram. Soc. Jpn 124 (2016) 870 – 874

[15] Gong J.F., Meng F.M., Fan Z.H., Li H.J. and Du Z., Template-free controlled hydrothermal synthesis for monodisperse flowerlike porous CeO_2 microspheres and their superior catalytic reduction of NO with NH_3, J. Alloys Comp. 690 (2017) 677 – 687

[16] Dastpak M., Farahmandjou M. and Firoozabadi T.P., Synthesis and preparation of magnetic Fe-doped CeO_2 nanoparticles prepared by simple sol-gel method, J. Supercond. Nov. Magn. 29 (2016) 2925 – 2929

[17] Lv Z.J., Zhong Q. and Ou M., Utilizing peroxide as precursor for the synthesis of CeO_2/ZnO composite oxide with enhanced photocatalytic activity, Appl. Surf. Sci. 376 (2016) 91 – 96

[18] Leino E., Kumar N., Maki-Arvela P., Aho A., Kordas K., Leino A.R., Shchukarev A., Murzin D.Y. and Mikkola J.P, Influence of the synthesis parameters on the physico-chemical and catalytic properties of cerium oxide for application in the synthesis of diethyl carbonate, Mater. Chem, Phys. 143 (2013) 65 - 75

[19] Vimal G., Mani K.P., Biju P.R., Joseph C., Unnikrishnan N.V. and Ittyachen M.A., Structural studies and luminescence properties of CeO_2:Eu^{3+} nanophosphors synthesized by oxalate precursor method, Appl. Nanoscience 5 (2015) 837 – 846

[20] Matei C., Covaliu C.I., Vasile B.S. and Berger D., Synthesis of ceria nanoparticles with controlled morphology, Romanian J. Mater. 44 (2014) 74 – 78

[21] Singh S., Srivastava P., Kapoor I.P.S. and Singh G., Preparation, characterization, and catalytic activity of rare earth metal oxide nanoparticles Part 84, J. Thermal Anal. Calorim. 111 (2013) 1073 – 1082

[22] Masuda Y., Thermal decomposition of formates. Part IX. Thermal decomposition of rare earth formate anhydrides, Thermochimica Acta 67 (1983) 271 - 285

[23] Fedorova I.V., Shchurov V.A., Fedorov A.A. and Gaisinovich M.S., Thermal-decomposition of formates of certain d-elements and f-elements, J. Appl. Chem. USSR 65 (1992) 587 - 591

[24] Arii T., Kishi A., Ogawa M. and Sawada Y., Thermal decomposition of cerium (III) acetate hydrate by a three-dimensional thermal analysis, Anal. Sci. 17 (2001) 875 - 880

[25] Arii T., Taguchi T., Kishi A., Ogawa M. and Sawada Y., Thermal decomposition of cerium (III) acetate studied with sample-controlled thermogravimetric-mass spectrometry (SCTG-MS), J. Eur. Ceram. Soc. 22 (2002) 2283 - 2289

[26] Ogawa M. and Manabe K., Formation of dilanthanide monoxide tetrapropionate by thermal-decomposition of propionate monohydrate of rare-earth elements (La, Ce, Pr, Nd), Nippon Kagaku Kaishi 5 (1993) 617 - 622

[27] Roura P., Farjas J., Camps J., Ricart S., Arbiol J., Puig T. and Obradors X., Decomposition processes and structural transformations of cerium propionate into nanocrystalline ceria at different oxygen partial pressures, J. Nanoparticle Research 13 (2011) 4085 - 4096

[28] Paul R.C., Bains M.S. and Ghotra J.S., Studies un carboxylates of metals: Part III – Lanthanum & cerium(III) carboxylates, Indian J. Chem. 7 (1969) 514 - 517

[29] Lazareva L.S., Ambrozhii M.N. and Dvornikova L.M., Thermal stability of cerium and praseodymium valerates, Zh. Neorg. Khimii 15 (1970) 354 - 357

[30] Brzyska W. and Paszkowska B., Studies on the thermal decomposition of rare earth caproates, J. Thermal Anal. 51 (1998) 561 - 566

[31] Misra S.N., Misra T.N. and Mehrotra R.C., Organic salts of lanthanide elements – I Preparation of tri-acylates of lanthanum and cerium(III) from aqueous solutions, J. Inorg. Nucl. Chem. 25 (1963) 195 - 199

[32] J.-C. Grivel, N.H. Andersen, P.G.A.P. Pallewatta, Y. Zhao and M. von Zimmermann, Influence of Bi, Se and Te additions on the formation temperature of MgB_2, Supercond. Sci. Technol. 25 (2012) 015010 (6pp)

[33] J.-C. Grivel, A.C. Wulff, Y. Zhao, J. Bednarčik and M. V. Zimmermann, In situ study on the formation of FeTe, J. Mater. Sci. 46 (2011) 4540 – 4544

[34] Mehrotra K.N., Chauhan M. and Shukla R.K., Infrared, thermal and X-ray diffraction analysis of cerium soaps, Tenside Surfactants Detergents 34 (1997) 124 - 127

[35] Grivel J.C., Suarez Guevara M.J., Attique F., Zhao Y., Tang X. Pallewatta P.G.P.A., Watenphul A. and Zimmermann M.v., Thermal decomposition of yttrium(III) hexanoate in argon, J. Anal. Appl. Pyrolysis 112 (2015) 237 - 243

[36] Grivel J.C., Zhao Y., Suarez Guevara M.J. and Watenphul A., Studies on the thermal decomposition of lanthanum(III) valerate and lanthanum(III) caproate in argon, Thermochim. Acta 612 (2015) 1 - 9

[37] SDBS Web : http://sdbs.db.aist.go.jp (National Institute of Advanced Industrial Science and Technology, 2016)

[38] J.A.R. Cheda, M.V. García, M.I. Redondo, S. Gargani and P. Ferloni, Short chain copper(II) *n*-alkanoate liquid crystals, Liquid Crystals 31 (2004) 1 – 14

[39] Marques E.F., Burrows H.D. and Miguel M.D., The structure and thermal behavior of some long chain cerium(III) carboxylates, J. Chem. Soc. Faraday Trans. 94 (1998) 1729 - 1736

[40] Jongen L., Binnemans K., Hinz D. and Meyer G., Mesomorphic behaviour of cerium(III) alkanoates, Mater. Sci. Eng. C 18 (2001) 199 - 204

[41] Umemura J., Cameron D.G. and Mantsch H.H., An FT-IR study of micelle formation in aqueous sodium *n*-hexanoate solutions, J. Phys. Chem. 84 (1980) 2272 – 2277

[42] Deacon G.B., and Phillips R.J., Relationships between the carbon-oxygen stretching frequencies of carboxylate complexes and the type of carboxylate coordination, Coord. Chem. Rev. 33 (1980) 227–250

[43] Torres P., Norby P. and Grivel J.-C., Thermal decomposition of barium valerate in argon, J. Anal. Appl. Pyrolysis 116 (2015) 120 - 128

[44] Goldsmith J.A. and Ross S.D., Factors affecting infra-red spectra of some planar anions with D_{3h} symmetry. 3. Spectra of rare-earth carbonates and their thermal decomposition products, Spectrochim. Acta A 23 (1967) 1909 - 1915

[45] Grivel J.-C., Zhao Y., Tang X., Pallewatta P.G.P.A., Watenphul A. and Zimmermann M.v., Thermal decomposition of yttrium(III) valerate in argon, J. Anal. Appl. Pyrolysis 106 (2014) 125 – 131

[46] Grivel J.-C., Zhao Y., Tang X., Pallewatta P.G.P.A., Watenphul A. and Zimmermann M.v., Thermal decomposition of lanthanum(III) butyrate in argon atmosphere, Thermochimica Acta 566 (2013) 112 – 117

[47] Grivel J.-C., Thermal decomposition of yttrium(III) propionate and butyrate, J. Anal. Appl. Pyrolysis 101 (2013) 185 - 192

[48] Jongen L., Binnemans K., Hinz D., Meyer G., Thermal behavior of lanthanum(III) alkanoates, Liq. Cryst. 28 (2001) 1727–1733

[49] Jongen L., Binnemans K., Hinz D. and Meyer G., Mesomorphic behaviour of praseodymium(III) alkanoates, Liquid Crystals 28 (2001) 819 - 825

[50] Binnemans K., Jongen L., Broman C., Hinz D., Meyer G., Structure and mesomorphism of neodymium(III) alkanoates, Inorg. Chem. 39 (2000) 5938–5945

[51] Grivel J.-C., Zhao Y., Tang X., Pallewatta P.G.P.A. and Watenphul A., Thermal decomposition of heavy rare-rearth butanoates, $Ln(C_3H_7CO_2)_3$ (Ln = Er, Tm, Yb and Lu) in argon, J. Thermal Anal. Calorim. 126 (2016) 1111 - 1122

[52] Glasner A. and Steinberg M., Thermal decomposition of the light rare earth oxalates, J. Inorg. Nucl. Chem. 22 (1961) 39 - 48

[53] Ambrozini B., Dametto P.R., Siqueira A.B., Carvalho C.T. and Ionashiro M., Synthesis, characterization and thermal behavior of solid tartrates of light trivalent lanthanides, J. Therm. Anal. Calorim. 97 (2009) 761 - 764

[54] Brouca-Cabarrecq C. and Trombe J.-C., f-element croconates 1. Lanthanide croconates – synthesis, crystal structure and thermal behavior, Inorg. Chim. Acta 191 (1992) 227 - 240

[55] Brzyska W. and Ożga W., Thermal decompositions of lanthanum and lanthanide salts of sebacic acid, J. Thermal Anal. 37 (1991) 2573 – 2583

[56] Brzyska W. and Ożga W., Thermal decompositions of yttrium and lanthanide complexes with mephenamic acid, Thermochim. Acta 195 (1992) 149 – 155

[57] Caires F.J., Lima L.S., Gomes D.J.C., Gigante A.C., Treu-Filho O. and Ionashiro M., Thermal and spectroscopic studies of solid oxamate of light trivalent lanthanides, J. Therm. Anal. Calorim. 111 (2013) 349 - 355

[58] Gomes D.J.C., Caires F.J., Silva R.C., Treu-Filho O. and Ionashiro M., Synthesis, characterization, thermal and spectroscopic studies of solid glycolate of light trivalent lanthanides, except promethium, Thermochim. Acta 587 (2014) 33 - 41

[59] Kula A., Thermal decomposition of lanthanide(III) and Y(III) 3,4,5-trihydroxybenzoates, J. Thermal Anal. Calorim. 75 (2004) 79 - 86

[60] Lima L.S., Caires F.J., Carvalho C.T., Sequeira A.B. and Ionashiro M., Synthesis, characterization and thermal behavior of solid-state compounds of light trivalent lanthanide succinates, Thermochim. Acta 501 (2010) 50 - 54

[61] Locatelli J.R., Rodrigues E.C., Siqueira A.B., Ionashiro E.Y., Bannach G. and Ionashiro M., Synthesis, characterization and thermal behaviour of solid-state compounds of yttrium and lanthanide benzoates, J. Thermal Anal. Calorim. 90 (2007) 737 - 746

[62] Rzączyńka Z. and Bartyzel A., Synthesis and characterization of complexes of rare earth elements with 1,1-cyclobutanedicarboxylic acid, J. Thermal Anal. Calorim. 68 (2002) 937 - 949

[63] Tsymbarenko D.M., Martynova I.A., Malkerova I.P., Alikhanyan A.S. and Kuzmina N.P., Mixed ligand acetate, propionate, and pivalate complexes of rare earth metals with monoethanolamine: A new approach to the synthesis, composition, structure, and use for the preparation of oxide materials, Russ. J. Coord. Chem. 42 (2016) 662 - 678

Figure captions

Figure 1: FTIR spectrum of the as-prepared Ce-hexanoate, Ce-pentanoate and Ce-butanoate samples with band assignments based on [35,36,38,46].

Figure 2: In-situ high energy (synchrotron) XRD patterns recorded during heating Ce-hexanoate powders at 5°C/min in Ar.

Figure 3: DTA (a), TG (b) and DTG (c) traces recorded on Ce-hexanoate upon heating at 5°C/min in Ar. Lower inset in (a): detail of the DTA trace at low temperature; upper inset in (a): magnification of the DTA trace around 300°C.

Figure 4: Hot stage optical microscope pictures taken at various temperatures during heating under Ar flow at 5°C/min on powders initially consisting of Ce-hexanoate.

Figure 5: FTIR spectra of the solid residue quenched from various temperatures along a heating ramp of 5°C/min in an Ar atmosphere. The starting powders consisted of Ce-hexanoate.

Figure 6: In-situ high energy (synchrotron) XRD patterns recorded during heating Ce-hexanoate powders at 5°C/min in Ar. a: low 2θ angle range, b: high 2θ angle range. ● CeO_2; ◆ $Ce_2O_2CO_3$; ○ Ce_2O_3.

Figure 7: FTIR spectra of the gas phase evolved from Ce-hexanoate a different temperatures during thermal decomposition. ○ CO_2; ● $C_5H_{11}COC_5H_{11}$.

Figure 8: DTA (a), TG (b) and DTG (c) traces recorded on Ce-pentanoate upon heating at 5°C/min in Ar.

Figure 9: DTA (a), TG (b) and DTG (c) traces recorded on Ce-butanoate monohydrate upon heating at 5°C/min in Ar. Inset in (a): detail of the DTA trace at low temperature.

Figure 10: Comparison of the DTA traces of Ce-butanoate monohydrate, Ce-pentanoate and Ce-hexanoate between 190°C and 410°C.

Table caption

Table 1: Temperatures of the maximum of the DTA endothermic peaks I, II and IV as well as the temperature range for the disappearance of the absorption bands of alkanoate ligands in FTIR spectra of quenched samples.

Compound	I	II	IV	end of alkanoate ligand release
Ce butanoate	118±5°C	165.0±0.5°C	353.8±0.5°C	375°C – 385°C
Ce pentanoate	119.8±0.5°C	159.8±0.8°C	359.7±0.5°C	410°C – 420°C
Ce hexanoate	112.5±0.6°C	157.9±0.5°C	361.5±0.5°C	450°C - 460°C